Langmuir Turbulence and Surface Heating in the Ocean Surface Boundary Layer

BRODIE C. PEARSON* AND ALAN L. M. GRANT

University of Reading, Reading, United Kingdom

JEFF A. POLTON

National Oceanography Centre, Liverpool, United Kingdom

STEPHEN E. BELCHER

University of Reading, Reading, United Kingdom

(Manuscript received 26 January 2015, in final form 24 June 2015)

ABSTRACT

This study uses large-eddy simulation to investigate the structure of the ocean surface boundary layer (OSBL) in the presence of Langmuir turbulence and stabilizing surface heat fluxes. The OSBL consists of a weakly stratified layer, despite a surface heat flux, above a stratified thermocline. The weakly stratified (mixed) layer is maintained by a combination of a turbulent heat flux produced by the wave-driven Stokes drift and downgradient turbulent diffusion. The scaling of turbulence statistics, such as dissipation and vertical velocity variance, is only affected by the surface heat flux through changes in the mixed layer depth. Diagnostic models are proposed for the equilibrium boundary layer and mixed layer depths in the presence of surface heating. The models are a function of the initial mixed layer depth before heating is imposed and the Langmuir stability length. In the presence of radiative heating, the models are extended to account for the depth profile of the heating.

1. Introduction

The ocean surface boundary layer (OSBL) is mixed by turbulence, driven by a combination of surface waves, wind stress, and surface heat fluxes. Surface waves can result in mixing through wave breaking and through a ''vortex force'' interaction between the wave-induced Stokes drift (Stokes 1847) and the vorticity in the flow (Craik and Leibovich 1976). Instabilities created by this vortex force produce Langmuir turbulence, which is believed to be a significant contributor to upper-ocean mixing over the global ocean (Li et al. 2005; Belcher et al. 2012; D'Asaro 2014).

Heat fluxes into the ocean can be separated into shortwave radiative heating, where the radiation is absorbed over a depth of several meters (Denman 1973; Paulson and Simpson 1977), and surface heating (sensible and latent heating and longwave radiation). The OSBL often exhibits a strong diurnal cycle; during the day a shallow, weakly stratified (well mixed) layer is present, with a diurnal thermocline forming below this layer, and during the night a deeper convective well-mixed layer develops (Brainerd and Gregg 1993, 1995; Sutherland et al. 2013, 2014).

Large-eddy simulation (LES) has been used to study Langmuir turbulence, beginning with the work of Skyllingstad and Denbo (1995). Results from LES show that Langmuir turbulence can maintain weak stratification near the ocean surface in the presence of surface heating (Min and Noh 2004) and a diurnal thermocline in the presence of radiative and surface heating (Noh et al. 2009). Kukulka et al. (2013) showed that LES provides better agreement with observations of the diurnal cycle of upper-ocean temperature structure when the vortex force is included. In particular, in the daytime

* Current affiliation: Department of Earth, Environmental and Planetary Sciences, Brown University, Providence, Rhode Island.

Corresponding author address: B. Pearson, Dept. of Earth, Environmental and Planetary Sciences, Brown University, Box 1846, 324 Brook Street, Providence, RI 02912.
E-mail: brodie_pearson@brown.edu

DOI: 10.1175/JPO-D-15-0018.1

© 2015 American Meteorological Society

OSBL the stratification in an LES without Langmuir turbulence was greater than the observed stratification during periods of the Surface Waves Process Program (SWAPP) experiment, and including Langmuir turbulence in the LES reduced the stratification. The K-profile parameterization (KPP) model (Large et al. 1994) and the Price–Weller–Pinkel (PWP) model (Price et al. 1986), which are both popular OSBL models, produced stratification similar to the LES without Langmuir turbulence. Plueddemann and Weller (1999) showed that Langmuir circulations, which are structures associated with the presence of Langmuir turbulence, were present over the observation period simulated by Kukulka et al. (2013). They also showed that in periods of weak winds, where no Langmuir circulations were present, the observed stratification was similar to that obtained from the PWP model. Despite the previous LES studies, the structure of Langmuir turbulence in the presence of surface heating has not been investigated in detail and, as a result, the response of the wave-driven OSBL to a surface heat flux is not understood quantitatively.

In this study, LES is used to investigate the equilibrium structure of the wave-driven OSBL following the application of surface heating to an initially neutral OSBL. The study is confined to the OSBL driven by waves through the vortex force, rather than other wave effects such as wave breaking (Noh et al. 2004; Sullivan et al. 2007) and wave-induced nonbreaking turbulence (Babanin 2006). The goal of this work is to develop scalings for various OSBL properties, in particular the depth of the OSBL, and the profiles of dissipation and vertical velocity variance. For this reason, we principally investigate simulations with constant forcing that have reached equilibrium, rather than simulations of diurnal cycles or other transient scenarios. Focusing on idealized simulations also allows the effects of surface and shortwave radiative heating to be separated and compared. After a brief discussion of model details in section 2, the structure of the equilibrium OSBL is studied in section 3 using the budgets for the turbulence kinetic energy (TKE) and the turbulent heat flux. The variation in the depth of the OSBL with surface heating is investigated in section 4. The effects of shortwave radiative heating on the equilibrium mixed layer depth are investigated in section 5, and the resulting model is compared with an LES with diurnal radiative heating.

2. Model and simulations

The simulations use the Met Office Large Eddy Model (LEM). The LEM for atmospheric boundary layer studies is described in Shutts and Gray (1994). The modifications of the model to simulate the OSBL are described by Grant and Belcher (2009). These modifications include imposing a Stokes drift, which affects the momentum budgets through the vortex force, the Coriolis–Stokes force, and a modified pressure (Craik and Leibovich 1976; McWilliams et al. 1997). The Stokes drift profile is given by $\mathbf{u}_s = u_s\hat{\mathbf{x}} = u_{s0}\exp(z/\delta)\hat{\mathbf{x}}$, where u_{s0} is the surface Stokes drift; z is depth (negative); δ is the Stokes penetration length (positive), which is related to the wavelength of surface waves by $\delta = \lambda/(4\pi)$; and $\hat{\mathbf{x}}$ is a unit vector aligned with the x axis. The turbulent Langmuir number $\mathrm{La}_t = (u_*/u_{s0})^{1/2}$, where u_* is the surface friction velocity of the water (McWilliams et al. 1997), can be used to characterize the turbulence in the presence of wind and wave forcing. For equilibrium wind seas, $\mathrm{La}_t = 0.3$ (Li et al. 2005).

The model domain is 256 m × 256 m in the horizontal (x, y) and 90 m in the vertical (z), with resolutions of 2 and 0.6 m in the horizontal and vertical, respectively. The forcing for the following simulations was chosen so that the boundary layer turbulence was resolved, with the shallowest simulated boundary layers being just over 10 m deep. The resolution probably begins to have an effect in the shallowest mixed layers, but the resolved turbulent fluxes are much greater than the subgrid fluxes in all the simulations. The domain is horizontally doubly periodic. A damping layer is imposed below 65 m to damp gravity waves and prevent their reflection off the lower boundary.

Simulations are started from rest with a constant temperature layer, below which the fluid has constant stratification. All simulations are forced using a surface wind stress aligned with the x axis, with $u_* = 6.1 \times 10^{-3}\,\mathrm{m\,s^{-1}}$, equivalent to a 10-m wind speed of approximately $5\,\mathrm{m\,s^{-1}}$. The effects of rotation are included through the Coriolis parameter f. In all simulations, $\mathrm{La}_t = 0.3$.

In the surface heating simulations, the surface heat flux is initially zero, which allows Langmuir turbulence to develop a neutral boundary layer. After 50 000 s, the surface heat flux is increased linearly to a value H_0 over 5000 s and is held constant for the remainder of the simulation. The simulations are then continued until the turbulence statistics and boundary layer depth reach an equilibrium, and the flow statistics are then averaged over 40 000 s. The depth of the neutral mixed layer at 50 000 s is defined as the initial mixed layer depth h_i. The introduction of heating to an initially neutral boundary layer in these simulations is intended to be analogous to the morning transition of the diurnal cycle.

This study uses seven sets of surface heating simulations, shown in Table 1. Simulations with different values of f were carried out representing strong (SS), moderate (SM), weak (SW), and no rotation effects (SN). Surface heating simulations with a larger Stokes penetration length (SD) and a shallower initial mixed

TABLE 1. Forcing parameters for the surface heating simulations. Shown are the simulation set abbreviation, surface heat flux H_0, Langmuir stability length L_L, Coriolis parameter f, Stokes drift penetration length δ, and the initial mixed layer depth h_i. Note that the highest values of L_L correspond to the lowest values of H_0.

	H_0 (W m^{-2})	L_L (m)	f (s^{-1})	δ (m)	h_i (m)
SS	16–64	248–62	1.4×10^{-4}	4.8	53
SM	8–64	496–62	10^{-4}	4.8	53
SW	16–64	248–62	0.5×10^{-4}	4.8	53
SN	8–64	496–62	0	4.8	53
SD	16, 64	248, 62	10^{-4}	14.4	53
SH	10.6–42.6	372–93	10^{-4}	4.8	36
Neutral	0	∞	10^{-4}	4.8	53

layer (SH) were also carried out. A reference (neutral) simulation was carried out with no surface heat flux, and all other parameters were identical to the SM simulations. Also shown in Table 1 are the values of Langmuir stability length, $L_L = -w_{*L}^3/B_0$, where $B_0 = -\alpha g H_0/(\rho c_p)$ is the surface buoyancy flux, α is the thermal expansion coefficient, g is gravitational acceleration, and c_p is the specific heat capacity of water (Belcher et al. 2012). The range of heat fluxes across the simulations is 0–64 W m^{-2}, which is significantly smaller than the typical daytime maximum heating. However, we are interested in the scaling of Langmuir turbulence, and scaling laws should be general for a given turbulent flow, providing the flows span the same nondimensional parameter space. Using weak surface forcing allows us to carry out a large number of simulations, spanning a wide range of parameter space. The nondimensional parameter space of these simulations includes reasonable heating (~500 W m^{-2}) with moderate to strong winds (10-m wind speed > 10 m s^{-1}) and wind waves.

3. Results

The following section begins with a discussion of the profiles of mean temperature and turbulent heat flux with surface heating and the definition of the mixed layer depth. Following this, the turbulence and mean properties of the OSBL are investigated using a nondimensional framework.

a. Structure of the OSBL

Figure 1a shows the profiles of mean temperature $\overline{\theta}$ for two of the SM simulations, where overbars represent horizontal and temporal averages. The stratification $\partial\overline{\theta}/\partial z$ is small near the surface in both simulations, and the depth of the layer of weak stratification decreases as L_L becomes smaller. Below the weakly stratified layer is a temperature jump, with a second weakly stratified layer below. The initial model stratification is below 53 m.

Figure 1b shows the turbulent heat flux $\overline{w'\theta'}$ for the same simulations, where primed quantities denote the turbulent deviation from the mean of a variable. The heat flux varies linearly in a layer close to the surface, indicating that the stratification within this layer does not change with time (since $\partial\overline{\theta}/\partial t$ is uniform with depth). The mixed layer depth is defined by fitting a line to the $\overline{w'\theta'}$ profiles near the surface, using the surface heat flux as a boundary condition. The mixed layer depth h_m is then defined as the depth at which the line reaches zero. The layer of weak stratification near the surface is within the mixed layer (Fig. 1a). Below h_m the turbulent heat flux is still nonzero, indicating that the boundary layer depth h_b, where the flux goes to zero, is greater than h_m.

The temperature jump between the surface and 53 m does not exceed 0.1 K in any of the simulations, despite more than 20 h of heating, indicating that commonly

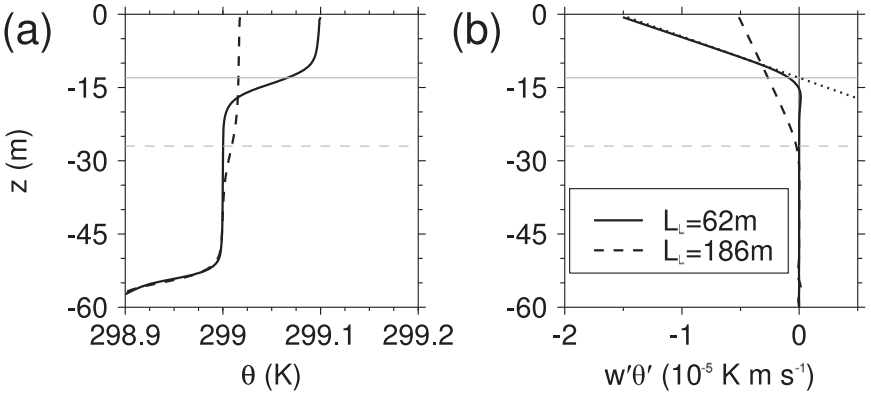

FIG. 1. Profiles of (a) mean temperature $\overline{\theta}$ and (b) turbulent heat flux $\overline{w'\theta'}$ from SM simulations with $L_L = 62$ m (solid) and $L_L = 186$ m (dashed). Horizontal gray lines show the mixed layer depth h_m for the simulation with the corresponding line style. The dotted line in (b) shows a linear fit to the $\overline{w'\theta'}$ profile within the mixed layer for $L_L = 62$ m. Note that by definition the dotted line intercepts the depth axis at h_m.

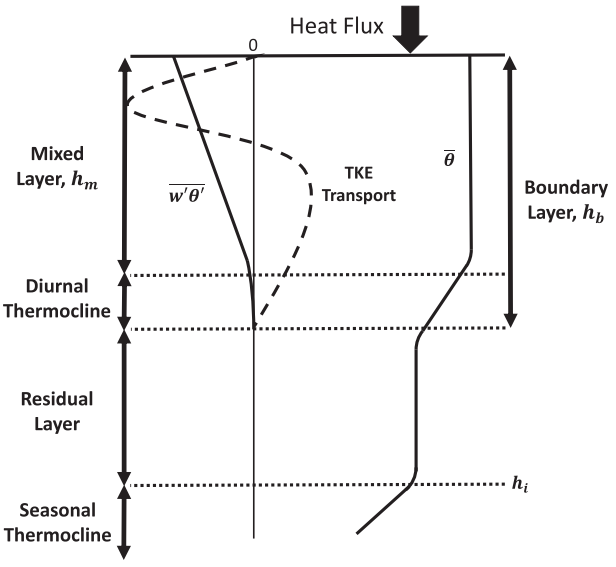

FIG. 2. Schematic of the separate layers in the upper ocean with surface heating. The boundary layer is the region containing surface-driven turbulence. The boundary layer can be separated into a mixed layer, where local temperature gradients are weak and approximately constant with time, and a diurnal thermocline, where the temperature gradient increases with time. The residual layer is detached from the surface and contains decaying turbulence, which remains from the initial boundary layer of depth h_i that was present before the introduction of heating. Below h_i is the seasonal thermocline, where the fluid is strongly stratified.

used definitions of the mixed layer using temperature or density jumps (e.g., de Boyer Montégut et al. 2004) would not be sufficient for diagnosing the depth of the turbulent mixed layer in these simulations.

Figure 2 shows a schematic of the equilibrium structure of the upper ocean in LES with surface heating. The new thermocline is a layer containing turbulent, stratified flow below the mixed layer. Despite the simulations being run to equilibrium, we refer to this layer as the diurnal thermocline, as in these simulations it is analogous to the thermocline that is formed and eroded over the course of a diurnal cycle. The boundary layer consists of the mixed layer and the diurnal thermocline, and the boundary layer depth h_b is defined as the maximum depth to which TKE is transported by the turbulence (Fig. 5d). The residual layer is the layer of weak stratification below the boundary layer, and it contains decaying turbulence, present before the surface heat flux was introduced. When the heating is introduced, the turbulence below h_b becomes detached from the surface. The time scale of this detachment in the present simulations is approximately 30 min, as shown in the appendix. The initial stratification imposed in the LES remains at depths below h_i.

Figure 3 shows the mean profiles of along-wind current $\overline{U}$ and crosswind current $\overline{V}$ for two SM simulations. The magnitudes of the along-wind and crosswind currents are largest near the surface. The along-wind current shear $\partial\overline{U}/\partial z$ is small near the surface, and this region of small $\partial\overline{U}/\partial z$ becomes shallower as the heating increases, because the boundary layer becomes shallower.

Figure 4 shows the resolved turbulent fluxes of momentum $\overline{u'w'}$ and $\overline{v'w'}$ and heat $\overline{w'\theta'}$ within the mixed layer normalized by the surface fluxes, with depth normalized by the mixed layer depth. The turbulent momentum fluxes (Fig. 4a) are almost entirely confined to the mixed layer. As L_L decreases, the $\overline{u'w'}$ profile becomes more linear and the magnitude of $\overline{v'w'}$ decreases. As the mixed layer becomes shallower, the parameter fh_m/u_* decreases, causing the curvature of the $\overline{u'w'}$ profile and the magnitude of $\overline{v'w'}$ to decrease (Grant and Belcher 2009).

The $\overline{w'\theta'}$ profiles are linear over most of the mixed layer because of the definition of h_m. Near the base of the mixed layer, the $\overline{w'\theta'}$ profiles become curved and the flux

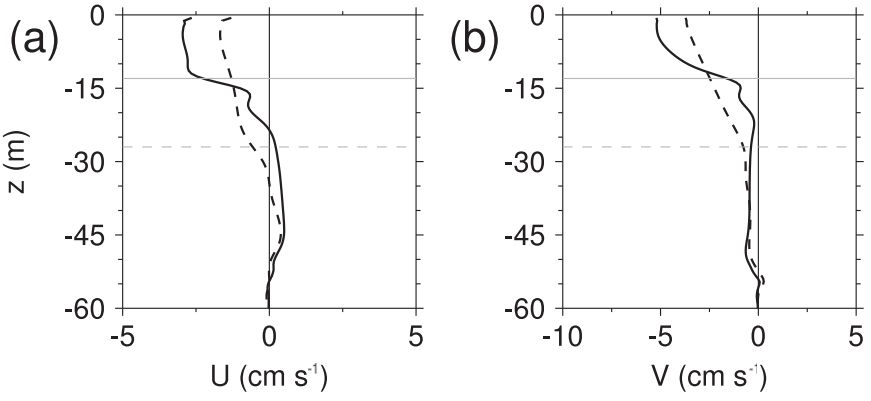

FIG. 3. Profiles of the (a) along-wind current $\overline{U}$ and (b) crosswind current $\overline{V}$ for SM simulations with $L_L = 62$ m (solid) and $L_L = 186$ m (dashed). Gray lines show the mixed layer depth for the simulation with the corresponding line style.

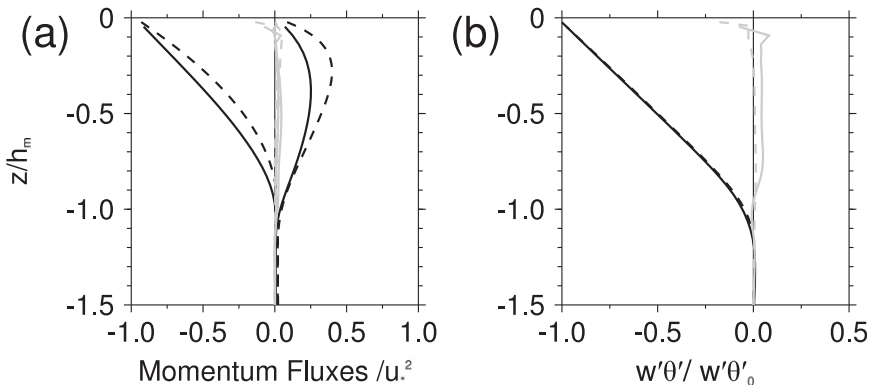

FIG. 4. Profiles of scaled turbulent fluxes of (a) along-wind $\overline{u'w'}/u_*^2$ (negative) and crosswind $\overline{v'w'}/u_*^2$ (positive) momentum and (b) heat $\overline{w'\theta'}\rho_0 c_p/H_0$ for SM simulations. Black lines show the total (resolved plus subgrid) fluxes, and gray lines show the subgrid component of the fluxes. Line styles correspond to $L_L = 62$ m (solid) and $L_L = 186$ m (dashed).

extends into the diurnal thermocline. The magnitude of subgrid fluxes of heat and momentum are much smaller than the resolved fluxes within the mixed layer.

b. Turbulent kinetic energy budget

For stationary turbulence under horizontally homogeneous conditions, the TKE budget in the presence of wave effects is (McWilliams et al. 1997; Polton and Belcher 2007)

$$0 = -\overline{u'w'}\frac{\partial u_s}{\partial z} - \overline{\mathbf{u}'w'}\cdot\frac{\partial \overline{\mathbf{U}}}{\partial z} + \overline{w'b'} - \frac{\partial}{\partial z}\left(\overline{w'\mathbf{u}'\cdot\mathbf{u}'} + \frac{1}{\rho}\overline{w'p'}\right) - \varepsilon, \qquad (1)$$

where $\mathbf{u}'$ and $\overline{\mathbf{U}}$ are the turbulence and mean velocity vectors, respectively; $\overline{w'b'}$ is the buoyancy flux, where $b' = \alpha g\theta'$ is the buoyancy; p is pressure; and ε is the rate of dissipation of energy through molecular viscosity. The terms on the right-hand side of Eq. (1) are, from left to right, Stokes production, shear production, buoyancy flux, TKE transport, and dissipation. Grant and Belcher (2009) used LES to show that the velocity and length scales of the TKE budget in Langmuir turbulence are $w_{*L} = (u_*^2 u_{s0})^{1/3}$ and the mixed layer depth h_m, respectively.

Figure 5 shows the first four terms on the rhs of Eq. (1) for two SM simulations and the neutral simulation. All the terms have been scaled by w_{*L}^3/h_m. The Stokes term is the largest production term in the TKE budget and is significant over a larger fraction of the mixed layer for smaller L_L. The region of significant Stokes drift gradient, and hence Stokes production, is confined to a near-surface layer with depth $O(\delta)$. As L_L decreases, δ/h_m increases, causing the Stokes production to be present deeper into the mixed layer.

Shear production occurs over the entire mixed layer. In the neutral simulation, shear production has a local maximum at approximately $0.25h_m$. This local maximum moves deeper into the mixed layer as L_L decreases and is below the region of significant Stokes production. The scaled $\overline{w'b'}$ profiles do not collapse for the SM simulations. The stability parameter h_m/L_L (Belcher et al. 2012) increases with decreasing L_L, indicating that the fraction of TKE produced through Stokes production, which is then used to transport heat through the mixed layer, increases with increasing surface heat flux.

The TKE transport takes energy from near the surface, where Stokes production is largest, and redistributes this energy deeper in the mixed layer. The layer of negative TKE transport covers an increasing fraction of h_m as L_L decreases. In the SM simulations, the positive region of TKE transport penetrates below the mixed layer into the diurnal thermocline and to the base of the boundary layer (Fig. 2).

Figure 6 shows the scaled dissipation $\varepsilon h_m/w_{*L}^3$ for all SM simulations and the neutral simulation. Above $0.7h_m$ the scaled dissipation profiles collapse onto a single curve. This indicates that the effects of surface heating on dissipation profiles in the upper mixed layer are captured entirely by variations in h_m, and the scaled dissipation profiles are the same as for Langmuir turbulence with no surface heating. Near the base of the mixed layer, the scaled dissipation profiles show some variation as a result of changes in the TKE transport and shear production, although this spread is much less than the spread in the unscaled dissipation profiles shown by the shaded area. The dissipation below the mixed layer decreases less rapidly with depth in the simulations with surface heating than in the neutral simulation because of decaying turbulence in the residual layer.

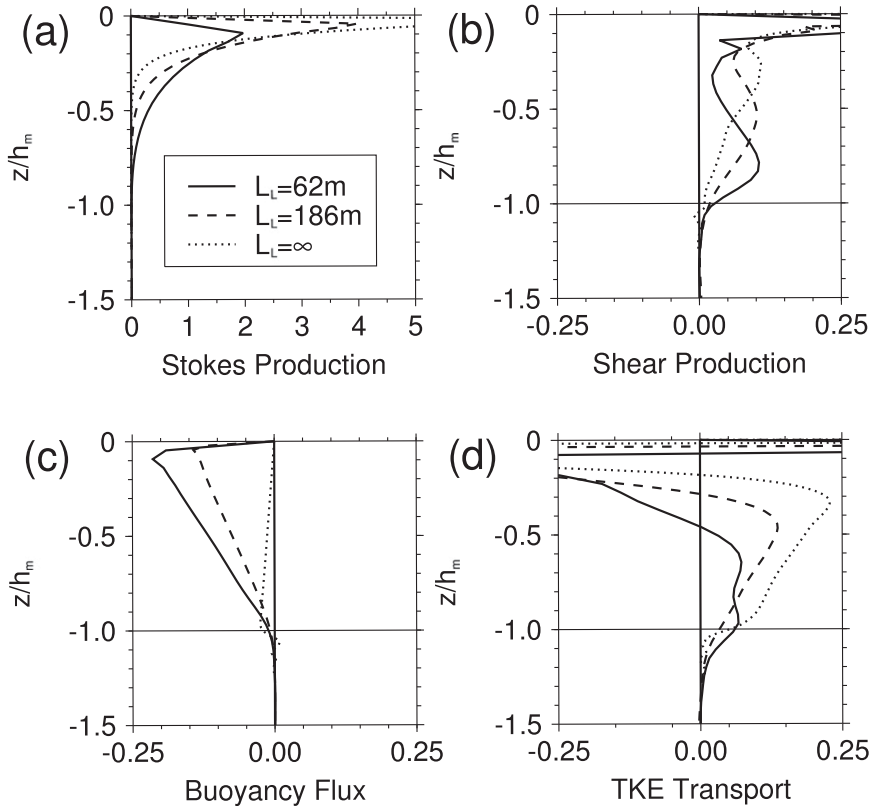

FIG. 5. Profiles of scaled terms in the TKE budget for SM simulations and a neutral simulation. Shown are (a) Stokes production, (b) shear production, (c) buoyancy flux, and (d) TKE transport. Shown are $L_L = 62$ m (solid), $L_L = 186$ m (dashed), and $L_L = \infty$ (dotted). All axes are made nondimensional using w_{*L} and h_m.

c. *Vertical velocity variance*

Figure 7 shows the profiles of vertical velocity variance σ_w^2 within the mixed layer for all SM and neutral simulations. The maximum of σ_w^2 near the surface is slightly smaller in the presence of surface heating than in neutral conditions. The peak in σ_w^2 is reduced by up to 25% across the SM simulations relative to the neutral simulation. The smallest σ_w^2 peaks are from the simulations with the smallest h_m, where the resolution could be beginning to affect the turbulence. The shape of the σ_w^2 profile above $0.7h_m$, neglecting the changes in magnitude, does not appear to be affected by the surface heat flux.

In the presence of surface heating, there is a significant increase in σ_w^2 around the base of the mixed layer due to gravity waves. These gravity waves contribute to σ_w^2 but do not dissipate energy, which is consistent with dissipation decreasing below $1.1h_m$, despite σ_w^2 being significant to a depth of at least $1.5h_m$ in some simulations.

d. *Heat flux budget*

There is greater stratification near the surface in shear-driven turbulence than in Langmuir turbulence (Noh et al. 2009; Kukulka et al. 2013). To understand why this is the case, we consider the budget for the turbulent heat flux.

The budget for the turbulent heat flux in a steady, horizontally homogeneous flow is given by

$$0 = -\sigma_w^2 \frac{\partial \overline{\theta}}{\partial z} - \overline{u'\theta'} \frac{\partial u_s}{\partial z} - \overline{\theta' b'} - \frac{1}{\rho} \overline{\theta' \frac{\partial p'}{\partial z}} - \frac{\partial \overline{w'w'\theta'}}{\partial z} - \varepsilon_{w\theta}, \tag{2}$$

where $\varepsilon_{w\theta}$ is the dissipation of $\overline{w'\theta'}$ through molecular viscosity and thermal diffusivity. The terms on the right-hand side of Eq. (2) are, from left to right, the gradient term, Stokes term, buoyancy term, pressure-scalar term, flux transport term, and flux dissipation. The scaling for terms in Eq. (2) is assumed to be $H_0/(\rho_0 c_p \tau)$, where $\tau = h_m/w_{*L}$ is a characteristic time scale for the turbulence.

Figure 8 shows the scaled profiles of the first four terms on the right-hand side of Eq. (2) within the mixed layer for the SM simulation with $L_L = 62$ m. From the surface to $0.8h_m$, the downward flux of heat is maintained by the Stokes and gradient terms in Eq. (2). The magnitude of the Stokes and gradient terms are comparable,

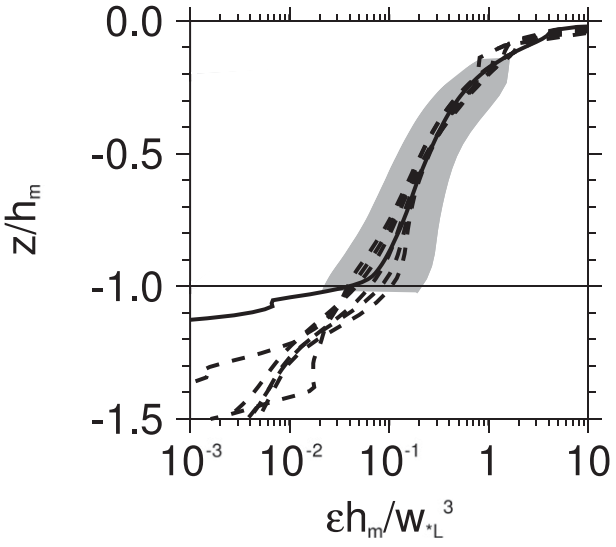

FIG. 6. Profiles of scaled dissipation of TKE $\varepsilon h_m/w_{*L}^3$ against z/h_m for all SM simulations (dashed) and a neutral simulation (solid). The shading shows the range in the profiles of unscaled dissipation.

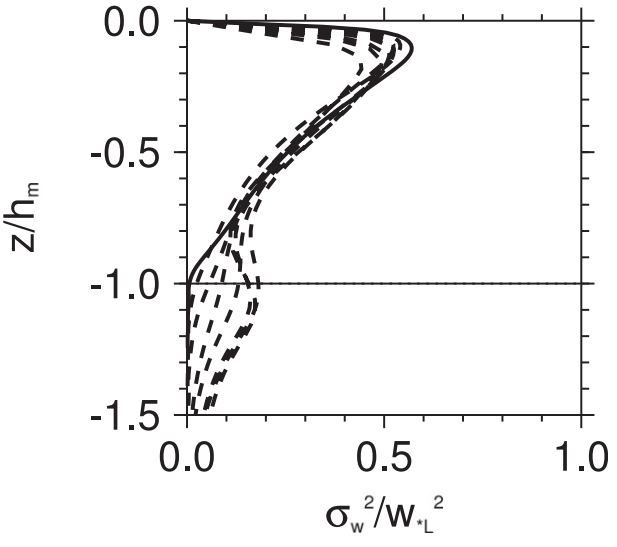

FIG. 7. Profiles of scaled vertical velocity variance σ_w^2/w_{*L}^2 for all SM simulations (dashed) and a neutral simulation (solid).

with the Stokes term being the larger of the two. The pressure-scalar and buoyancy terms balance the Stokes and gradient terms in the upper half of the mixed layer. The flux transport and flux dissipation are not shown in the figure. In these simulations $\varepsilon_{w\theta}$ is small, because the fluxes are carried by the largest eddies rather than parameterized subgrid eddies, and the flux transport is small. Near the base of the mixed layer, where the heat flux is small, the downward flux tendency of the pressure-scalar and gradient terms balances the buoyancy term, which is consistent with the presence of gravity waves.

Kukulka et al. (2013) argued that parameterizations of Langmuir turbulence should include the effects of Stokes drift on TKE production. Our results show that parameterizations should also include the effects of Stokes drift on the production of $\overline{w'\theta'}$, as we are about to explain.

The budget for the turbulent heat flux is the basis for the nonlocal component of the KPP scheme in unstable conditions (Holtslag and Moeng 1991), and it explains the countergradient transport of heat observed in the convective atmospheric boundary layer. The nonlocal part of the scheme, which allows countergradient transport, arises from the source terms in the $\overline{w'\theta'}$ budget that are not a function of the temperature gradient (Deardorff 1972). For stable conditions it is usually assumed that the only source in the $\overline{w'\theta'}$ budget is the gradient term, which implies simple downgradient transport ($\overline{w'\theta'} \propto \kappa_d \partial\overline{\theta}/\partial z$, where κ_d is a diffusivity). However, Fig. 8 shows that the Stokes term is an important source of $\overline{w'\theta'}$, and so its contribution to the transport of heat should also be represented as a nonlocal term in parameterizations for the turbulent heat flux. Note that the Stokes and gradient terms are both sources for the heat flux, reducing the temperature gradient needed for the same amount of heat transport compared to shear turbulence. This would be consistent with observations in the presence of Langmuir circulations (Plueddemann and Weller 1999). In addition, σ_w^2, which is related to κ_d, is larger in Langmuir turbulence than in shear-driven turbulence with the same surface

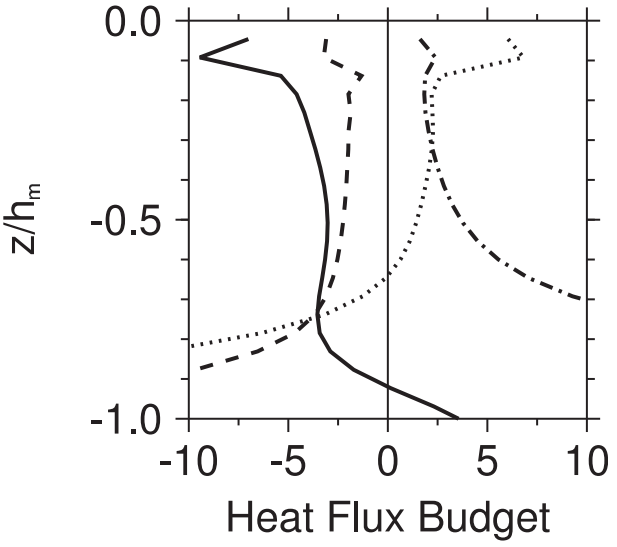

FIG. 8. Profiles of scaled terms in the $\overline{w'\theta'}$ budget [Eq. (2)] for the SM simulation with $L_L = 62$ m. Shown are the Stokes term (solid), gradient term (dashed), pressure-scalar term (dotted) and buoyancy term (dashed–dotted). All terms have been multiplied by $\tau\rho_0 c_p/H_0$.

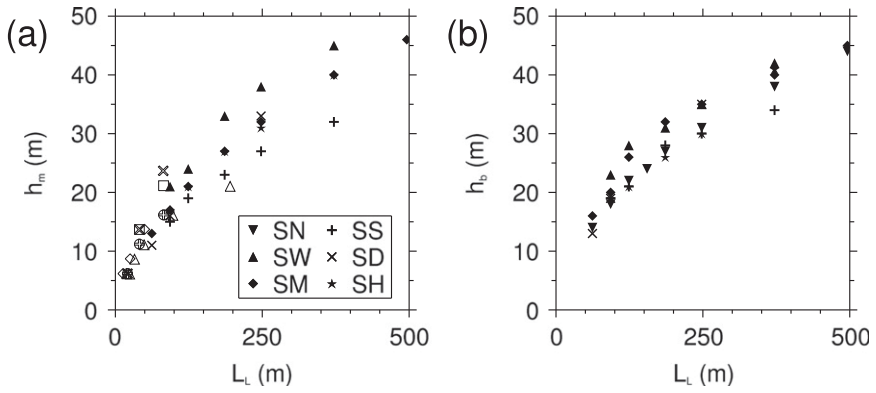

FIG. 9. Depths of the (a) mixed layer h_m and (b) boundary layer h_b as a function of L_L for all surface heating simulations. Filled symbols denote the simulation set. Open symbols show results from Min and Noh (2004). Mixed layer depths for the SN simulation are plotted in (b) because of the presence of a stratified shear layer (see text).

friction velocity (McWilliams et al. 1997; Teixeira and Belcher 2002, 2010).

4. The equilibrium depth of the mixed layer and boundary layer

The depths of the mixed layer and the boundary layer are important for the development of OSBL parameterizations as they describe the length scales of turbulence. In addition, h_b controls the heat capacity of the OSBL and hence the variation of the sea surface temperature in response to a surface heat flux. The formation of an equilibrium OSBL in the presence of Langmuir turbulence and surface heating indicates that h_m and h_b could be diagnosed from the forcing used in the simulations.

The values of h_m and h_b for the equilibrium OSBL must be a function of the characteristic length scales of the turbulent flow. The length scales that are commonly used to characterize boundary layers under a stabilizing heat flux are the Ekman depth u_*/f (Rossby and Montgomery 1935) and the Obukhov length $L = -u_*^3/(\kappa B_0)$ (Monin and Obukhov 1954), where κ is the von Kármán constant. Diagnostic models for the depth of stable geophysical boundary layers are generally a combination of the Ekman depth and the Obukhov length (e.g., Zilitinkevich 1972; Garwood 1977; Zilitinkevich and Baklanov 2002; Zilitinkevich et al. 2002). As a result of the new velocity (u_{s0}) and length (δ) scales introduced by the presence of Stokes drift, additional length scales can be constructed for Langmuir turbulence such as the Langmuir–Ekman depth w_{*L}/f and the Langmuir stability length L_L.

Figure 9 shows h_m and h_b against L_L for all simulations with surface heating. The mixed layer and boundary layer become deeper as L_L increases within each set of simulations. Kukulka et al. (2013) suggested that an alternative stability length, $L_K = \delta \ln(L_L/\delta)$, could provide an estimator for h_m, but the results from the present simulations show that L_K is not a useful estimator for h_m. Increasing δ by a factor of 3 does not significantly affect h_m, indicating that h_m is more sensitive to changes in L_L than to changes in δ.

Both h_m and h_b show some dependence on f; the mixed layer becomes deeper as f decreases and u_*/f increases. Grant and Belcher (2011) showed that for large $u_*/(fh_m)$, a stratified shear layer forms at the base of the boundary layer. In the presence of a stratified shear layer, the heat flux is nonzero at the base of the layer mixed by Langmuir turbulence, and the flux extends through the stratified shear layer. This means that $\overline{w'b'}$ cannot be used to define h_m (as in Fig. 2) for small values of f. Grant and Belcher (2011) showed that, in the presence of a stratified shear layer, Langmuir turbulence is confined to the mixed layer, defined as the depth over which TKE is transported by the turbulence. For the SN ($f = 0$) simulations the mixed layer depth has been calculated using the TKE transport, but these h_m have been plotted in Fig. 9b, alongside the other depths defined through TKE transport. In the SN simulations the combined depth of the mixed layer and the shear stratified layer is the boundary layer depth, which does not reach a steady state (Grant and Belcher 2011) and is not relevant to the effects of heating on Langmuir turbulence. As a result, the values of h_b from the SN simulations are not plotted. Figure 9b indicates that L_L is the main control on h_b.

Dimensional consistency requires that h_m and h_b must depend only on length scales within the simulations. The boundary layer depth does not vary significantly over a range of $u_*/f = [44\,\text{m}, \infty]$ and $\delta = [4.8\,\text{m}, 14.4\,\text{m}]$, which indicates that L_L is the only length scale with a significant effect on the value of h_b that can be constructed from the surface forcing parameters in these simulations. However,

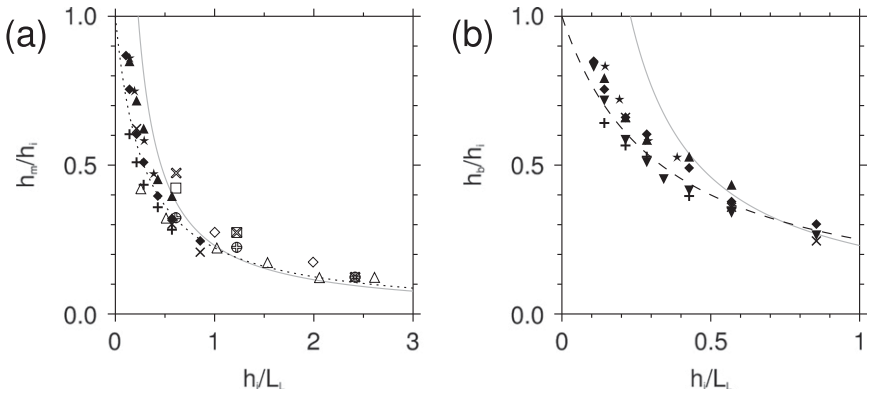

FIG. 10. Nondimensional depths of the (a) mixed layer h_m/h_i and (b) boundary layer h_b/h_i against the initial stability parameter h_i/L_L for all surface heating simulations. Symbols represent different sets of simulations, as in Fig. 9. The dotted line shows $h_m/h_i = [1 + 3.5(h_i/L_L)]^{-1}$, while the dashed line shows $h_b/h_i = [1 + 3.0(h_i/L_L)]^{-1}$. The gray lines show $h_m = 0.23L_L$ and $h_b = 0.23L_L$ in (a) and (b), respectively.

it is clear that a simple relationship of the form $h_b = \gamma L_L$, where γ is a constant, does not describe the variation in h_b.

The only length scale that has not been considered is the initial mixed layer depth h_i. Both h_m and h_b must asymptote toward h_i as L_L tends toward infinity. This indicates that h_i, along with L_L, could be responsible for the nonlinear variation of h_m with L_L seen in Fig. 9. In addition, for all L_L investigated here, simulations using $h_i = 36$ m have a smaller boundary layer depth than simulations using $h_i = 53$ m (note that in Fig. 9 the stars and diamonds indicate simulations that differ only in their values of h_i and L_L).

The initial mixed layer depth could affect the values of h_m and h_b through the turbulence present within the initial mixed layer. The introduction of surface heating adds a sink of TKE due to the buoyancy flux in Eq. (1). The largest, energy-containing, turbulent eddies are supplied with energy by Stokes production. The largest turbulent eddies are also responsible for the transport of heat and so lose energy through the buoyancy flux. As the mixed layer becomes shallower, the depth-averaged Stokes production increases as w_{*L}^3/h_m (Grant and Belcher 2009), resulting in the collapse of scaled dissipation profiles in Fig. 6. By noting that $\overline{w'b'}$ varies linearly with depth in the mixed layer, the buoyancy flux averaged over the mixed layer can be approximated by $B_0/2$. We assume that

$$\beta \frac{w_{*L}^3}{h_i} = \beta \frac{w_{*L}^3}{h_m} + \frac{B_0}{2}, \tag{3}$$

where β is a constant. Equation (3) can be rearranged to provide a relationship between the steady mixed layer depth and the initial mixed layer depth, as a function of the Langmuir stability length

$$\frac{h_m}{h_i} = \frac{1}{1 + (2\beta)^{-1}(h_i/L_L)}. \tag{4}$$

Figure 10a shows the nondimensional mixed layer depth h_m/h_i as a function of the initial stability parameter h_i/L_L for all surface heating simulations. The model of Eq. (4) shows good agreement with all of our simulations using $(2\beta)^{-1} = 3.5$. Figure 10b shows h_b/h_i against h_i/L_L. Also shown is Eq. (4), where h_m has been replaced by h_b, and $(2\beta)^{-1} = 3.0$, which provides a good fit to h_b for all the simulations. The boundary layer depths for simulations which differ only in h_i collapse better in Fig. 10b than in Fig. 9b.

The dependence of h_m and h_b on the initial mixed layer depth is an interesting result. As far as the authors are aware, the possibility that the depth of the initial boundary layer could affect the depth of an equilibrium stable boundary layer has not been recognized previously. This dependence on h_i means that it is not possible to create a diagnostic model for h_m and h_b that is based on only the instantaneous forcing parameters, although for $h_i/L_L \gg 1$, Eq. (4) tends to $h_m \propto L_L$. The relationship proposed in Eq. (4) is only valid for Langmuir turbulence $\mathrm{La}_t < 0.5$ (Grant and Belcher 2009).

Min and Noh (2004) carried out LES of the mixed layer with surface heating and estimated the mixed layer depth through tracer dispersion. The results of Min and Noh (2004) fit smoothly with our data (Figs. 9, 10). Thus, the model of Eq. (4) shows good agreement with the simulations of Min and Noh (2004) as well as with the current simulations.

5. Effects of radiative heating on mixed layer depth

In addition to the effects of surface heating, the ocean can also be stabilized by the absorption of shortwave

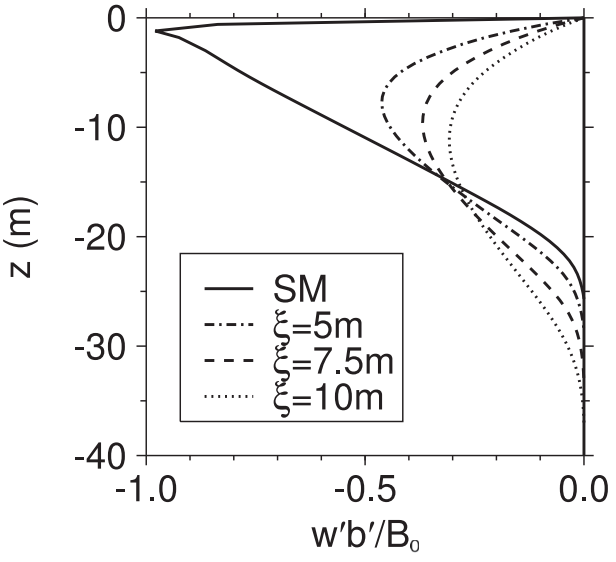

FIG. 11. Profiles of the scaled turbulent buoyancy flux $\overline{w'b'}/B_0$ for simulations with $L_L = 124$ m. The solid line is the SM simulation, while other line styles show simulations with varying radiative penetration depth ξ.

radiation, which can penetrate many meters into the water column. This shortwave radiative heating is an important source of ocean heating during the daytime. To investigate the effects of radiative heating on mixed layer depth, simulations are carried out that are identical to the SM simulations but replace the surface heat flux H_0 by an irradiance profile $I(z)$. The rate of heating due to the divergence of shortwave radiation is then given by $(\rho c_p)^{-1}\partial I(z)/\partial z$. The irradiance profile is chosen to be a simple exponential decay $I(z) = I_0 \exp(z/\xi)$, where I_0 is the surface irradiance and ξ is the radiative penetration length (Denman 1973). For the radiative heating simulations, we define a buoyancy flux, $B_0 = -\alpha g I_0/(\rho c_p)$, and use $L_L = 62$, 93, and 124 m and $\xi = 5$, 7.5, and 10 m.

Figure 11 shows profiles of the turbulent buoyancy flux for the radiative heating and SM simulations with $L_L = 124$ m. In the radiative heating simulations, the $\overline{w'b'}$ profiles are not linear but reach a minimum within the mixed layer. The depth of the $\overline{w'b'}$ minimum $h_{\rm rad}$ increases with increasing ξ. In addition to the changes in the shape of the $\overline{w'b'}$ profile, the depth of the mixed layer increases as ξ becomes larger.

Figure 12a shows the mixed layer depth as a function of L_L for radiative heating simulations compared with the results for the SM simulations [see Eq. (7) for definition of h_m in radiative heating simulations]. The mixed layer depth in the radiative heating simulations is up to 70% larger than the surface heating simulations with the same L_L. Similar variation was observed in h_b across the simulations (not shown). This variation in h_m indicates that while Eqs. (3) and (4) are applicable to surface heating, they do not apply for radiative heating. Ultimately, it is the turbulence that drives the dynamics of the OSBL, and the most obvious difference between OSBL turbulence for surface heating and for shortwave radiation is the $\overline{w'b'}$ profile (Fig. 11). In the presence of radiative heating, the $\overline{w'b'}$ profiles have several properties that are not present for surface heating. First, some radiation penetrates below the mixed layer, meaning that the divergence of the radiation within the mixed layer produces a buoyancy flux less than B_0, with the largest value $I(-h_m)/I_0 = 0.1$ for the present simulations. Second, the magnitude of the $\overline{w'b'}$ minimum, and hence the average turbulent buoyancy flux over the mixed layer, becomes smaller as ξ increases. Finally, radiative heating introduces a region where $\overline{w'b'}$ has a positive gradient above $h_{\rm rad}$.

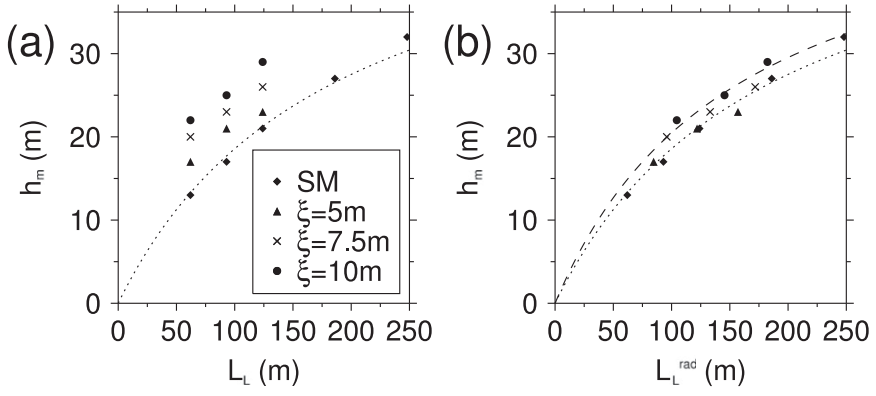

FIG. 12. Mixed layer depths plotted against (a) Langmuir stability length L_L and (b) radiative Langmuir stability length $L_L^{\rm rad}$ [Eq. (5)] for radiative heating and SM simulations. Symbols indicate the simulation set and the radiative penetration depth ξ. The lines show $y = h_i/[1 + (2\beta)^{-1}(h_i/x)]$ with $(2\beta)^{-1} = 3.5$ (dotted) and 3 (dashed).

The mixed layer depths were found to collapse better across the simulations when plotted as a function of L_L^{rad} rather than L_L, with

$$L_L^{\mathrm{rad}} = -\frac{w_{*L}^3}{B_0[1-\exp(-h_{\mathrm{rad}}/\xi)]} = -\frac{w_{*L}^3}{B_0^{\mathrm{rad}}}, \qquad (5)$$

where B_0^{rad} is an effective buoyancy flux. Figure 12b shows h_m as a function of L_L^{rad} for the radiative heating and SM simulations. The mixed layer depths for the radiative heating simulations show good agreement with Eq. (4) using L_L^{rad} in place of L_L. However, we found a better fit to the simulations with the largest ζ was achieved if $(2\beta)^{-1} = 3$. This indicates that while using L_L^{rad} in place of L_L improves the model fit to radiative heating simulations, there are further, smaller, radiative heating profile effects that could be investigated in the future. The collapse of boundary layer depths for all radiative heating simulations (not shown) when plotted against L_L^{rad} shows a spread similar to Fig. 12b. In the presence of radiation, Eq. (5) is equivalent to defining the relevant buoyancy flux B_0^{rad} using the radiative heating in the layer between the surface and the $\overline{w'b'}$ minimum. In the limit of ξ tending to zero, $L_L^{\mathrm{rad}} \to L_L$, which is equivalent to heating confined to a layer close to the surface, for example, because of radiation-absorbing material in the water column.

Combining Eqs. (4) and (5) results in an expression for h_m that depends on h_{rad}, a property of the turbulent flow. The value of h_{rad} can be approximated as a function of forcing parameters by considering the temperature budget. In the presence of radiative heating, the condition for the temperature gradient within the mixed layer to stay constant with time is

$$\alpha g \frac{\partial}{\partial z}\left(\frac{\partial \overline{\theta}}{\partial t}\right) = \frac{\partial^2}{\partial z^2}\left(\frac{\alpha g}{\rho c_p} I - \overline{w'b'}\right) = 0. \qquad (6)$$

Figure 13 shows that the sum of radiative and turbulent buoyancy fluxes is linear over most of the mixed layer. In this simulation approximately 10% of the radiation penetrates deeper than the mixed layer and the radiative heat flux is comparable to the turbulent buoyancy flux over the mixed layer. By noting that the irradiance profile is known, and assuming that the turbulent heat flux tends to zero at the surface and base of the mixed layer, Eq. (6) can be integrated over the mixed layer to give

$$\overline{w'b'}(z) = B_0\left[1 - e^{z/\xi} + \frac{z}{h_m}(1 - e^{-h_m/\xi})\right]. \qquad (7)$$

The value of h_m in the radiative heating simulations is found by fitting Eq. (7) to the $\overline{w'b'}$ profiles in the upper ocean, which is equivalent to setting the sum of $\overline{w'b'}$ and the irradiance to vary linearly with depth within the mixed layer. Figure 13 shows that Eq. (7) agrees well over most of the mixed layer with the turbulence buoyancy flux profile for a simulation using $\xi = 10$ m and $L_L = 124$ m. The turbulent buoyancy flux deviates from Eq. (7) near the base of the mixed layer and penetrates below h_m, although the majority of the total buoyancy flux through the mixed layer base is a result of the radiation penetrating beyond the mixed layer.

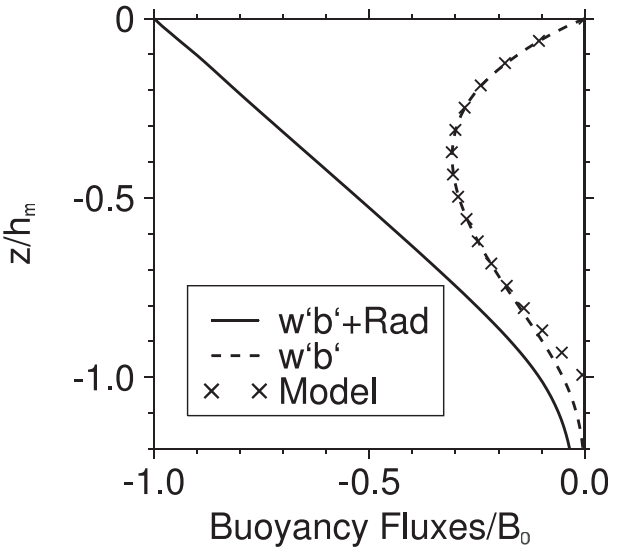

FIG. 13. Profiles of components of the total buoyancy flux against nondimensional depth for a radiative heating simulation with $\xi = 10$ m and $L_L = 124$ m. The solid line shows the total buoyancy flux $[\overline{w'b'} - \alpha g I(z)/(\rho c_p)]/B_0$, the dashed line shows the turbulent buoyancy flux $\overline{w'b'}/B_0$, and the crosses show the model of Eq. (7) with $h_m = 29$ m.

Equation (7) can be differentiated to find the depth of the $\overline{w'b'}$ minimum

$$h_{\mathrm{rad}} = -\xi \ln\left[\frac{\xi}{h_m}(1 - e^{-h_m/\xi})\right]. \qquad (8)$$

Diagnosing the steady mixed layer depth under radiative or surface heating using Eq. (4), and replacing L_L by L_L^{rad} [Eqs. (5) and (8)], only requires four parameters: B_0, h_i, w_{*L}, and ξ. These parameters depend only on the surface forcing and the bulk OSBL properties, allowing h_m to be diagnosed.

In the real world the divergence of shortwave radiation contains several distinct decay depths (Paulson and Simpson 1977). The results of this idealized study indicate that the equilibrium mixed layer depth in the presence of a more realistic heating profile will be a weighted function of the individual decay depths and the surface forcing conditions.

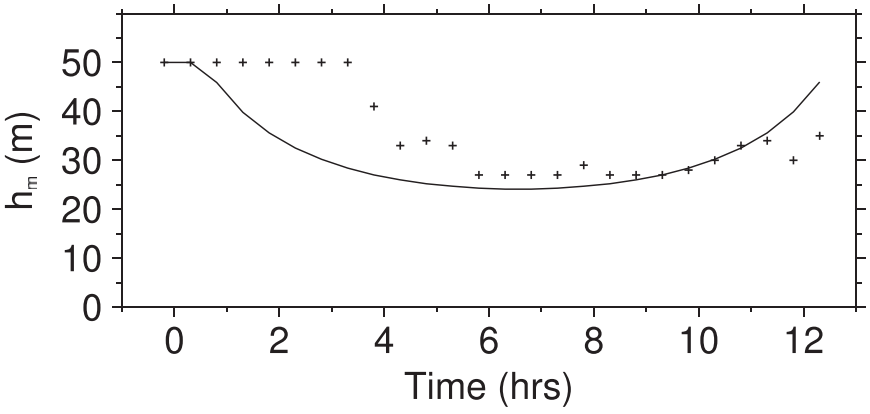

FIG. 14. A comparison between LES mixed layer depth and the parameterized mixed layer depth for a diurnal radiative heating simulation. The radiative heating begins at time zero. The crosses indicate the mixed layer depth in the LES, diagnosed from the turbulent buoyancy flux. The line shows $h_m = h_i/[1 + 3(h_i/L_L^{\text{rad}})]$, where L_L^{rad} is calculated using the instantaneous radiative heating profile.

The diurnal cycle

The results in Fig. 12, and the parameterization for mixed layer depth given by Eqs. (4) and (5), were obtained for steady-state conditions. However, during the daytime the solar radiation varies with time, and it is of interest to see how well our diagnostic parameterization represents the daytime variation in mixed layer depth.

To investigate this, an LES was carried out using time-varying radiation. A neutral boundary layer was allowed to develop and then solar radiation, varying sinusoidally with a period of 24 h, was applied for 12 h (the heating phase of the sinusoid). The maximum irradiance was 64 W m^{-2}, the radiative decay depth was $\xi = 10$ m, and $h_i = 50$ m. The mixed layer depth was determined from the heat flux profiles averaged over 1800 s.

Figure 14 compares the mixed layer depth from the LES with that calculated using the parameterization given in Eq. (4), with L_L replaced by L_L^{rad} [Eq. (5)] and $(2\beta)^{-1} = 3$, as suggested by Fig. 12. The parameterized h_m starts to decrease when the irradiance starts to increase and reaches a minimum when the irradiance is greatest. For the first 3 h after the irradiance becomes positive, the mixed layer depth in the LES remains constant at the initial depth. After 3 h, h_m in the LES decreases with time until it is similar to the parameterized mixed layer depth.

The turbulence time scale for the initial neutral boundary layer, $\tau = h_i/w_{*L}$, is approximately 1 h. This suggests that some of the delay before the mixed layer depth decreases in the LES is associated with the evolution of the turbulence that occurs on a time scale τ (see appendix). The diagnostic parameterization gives a reasonable prediction of the minimum mixed layer depth, but further work is needed to understand how the mixed layer depth varies in time.

Starting around 9 h, the parameterized mixed layer depth begins to increase as the radiation decreases, while the LES shows h_m remaining around 30–35 m. Since the parameterization depends on the instantaneous irradiance, it will give the same depth for increasing or decreasing heat flux. This means that the variation in the parameterized h_m is symmetric about the time of maximum irradiance. However, the boundary layer warms through the day and this will affect the evolution of mixed layer depth as the irradiance decreases with time.

In this study, the effects of surface fluxes and radiation have been considered separately. However, to simulate a realistic diurnal cycle, it is necessary to represent situations in which surface fluxes and radiation are present together. Typically, the surface flux will represent a loss of heat from the ocean and have the opposite sign to the solar radiative flux. In addition, the present study has only considered simple exponential radiation profiles, but the profile of absorption of radiation in the ocean is more complex. Further work is needed to understand the behavior of the mixed layer depth in more realistic situations.

6. Conclusions

This study has investigated the effects of surface heating on the ocean surface boundary layer (OSBL) driven by Langmuir turbulence. Large-eddy simulations were used to study the structure and equilibrium depth

of the OSBL and mixed layer following the introduction of a constant surface heat flux to a neutral OSBL. The simulations cover a range of nondimensional parameter space that includes moderate to strong winds (10-m wind speed $\geq 10\,\mathrm{m\,s^{-1}}$) with wind waves and moderate surface heating ($\sim 500\,\mathrm{W\,m^{-2}}$) or weak winds and waves under weak surface heating.

In the presence of surface heating, the LES produces an OSBL consisting of a weakly stratified (mixed) layer near the surface, above a stratified thermocline, consistent with observations. The mixed layer is maintained by Langmuir turbulence, which produces a turbulent heat flux through the layer for two reasons. First, the Stokes drift transports heat down the Stokes drift gradient (away from the surface), regardless of the stratification. Second, the large vertical velocity variances σ_w^2 in Langmuir turbulence allow the turbulence to transport heat downgradient more efficiently than in shear-driven turbulence, where stronger stratification develops near the surface (Kukulka et al. 2013).

The dissipation ε and σ_w^2 profiles in Langmuir turbulence with surface heating were found to scale with w_{*L} and h_m, the same scaling as Langmuir turbulence without surface heating (Grant and Belcher 2009). This means that surface heating only affects equilibrium ε and σ_w^2 profiles through changes to the mixed layer depth.

The equilibrium depths of the mixed layer h_m and boundary layer h_b were found to be a function of the Langmuir stability length L_L and the initial mixed layer depth h_i before the heat flux is introduced. The models for h_m and h_b developed here [Eq. (4)] are based on a depth-averaged energy balance for the largest scales of turbulent motion. Part of the average Stokes production, before heating is introduced, balances the sum of the increased average Stokes production and the energy used to redistribute heat after a surface heat flux is imposed. Equation (4) is successful for a range of rotation rates and Stokes penetration lengths, implying that h_i and L_L are the most significant length scales for the prediction of h_m and h_b. The values of h_m, from the simulations and Eq. (4), are consistent with previous LES studies (Min and Noh 2004).

Simulations were also carried out to investigate the effects of radiative heating on h_m and h_b. As radiation penetrates more deeply into the water column, the equilibrium mixed layer depth increases for the same surface irradiance. The effect of exponential heating profiles, with varying decay lengths, on h_m can be accounted for through a radiative Langmuir stability length L_L^{rad} [Eq. (5)]. The mixed layer depths for radiative and surface heating simulations converge to a single profile when plotted as a function of L_L^{rad}.

Most of the simulations used in this paper focus on the collapse of an initial turbulent mixed layer following the introduction of a constant surface heat flux and the equilibrium structure of this layer. These simulations are a simplified version of the morning transition of the diurnal cycle. Although the constant forcing is unrealistic in a diurnal cycle, it allows for reasonable averaging times and a simple diagnostic parameterization for the mixed layer depth. The diagnostic parameterization for mixed layer depth was compared to an LES using diurnally varying radiative heating. The minimum h_m in the LES was similar to that of the diagnostic parameterization. However, there was a lag between the radiative heat flux beginning and the LES mixed layer shoaling, which was not captured by the model.

The above results suggest that turbulence closure schemes should include Langmuir turbulence if they are to capture the structure and the depth of the OSBL over the diurnal cycle. Notably, Langmuir turbulence is necessary to explain the weakly stratified layer near the surface and the depths of the mixed and boundary layers. Further investigation is required to see whether the arguments that build Eq. (4) also apply to the surface-heated OSBL when wind and/or waves decrease, causing L_L and, presumably, h_m to decrease. In the current paper, all simulations have $\delta < h_m$. Further studies could investigate the effects of strong heating with very weak waves, where $\delta/h_m > 1$, as this nondimensional parameter could affect the scaling of Langmuir turbulence for very shallow mixed layers (Harcourt and D'Asaro 2008).

Acknowledgments. This work was supported by the NERC under the OSMOSIS project, Grant NE/I020083/1. In addition, J.A.P. was supported by NOC Grant NE/I01993X/1, and B.C.P. was partially supported by NSF OCE 1350795. Comments from two anonymous reviewers helped improve this paper.

APPENDIX

Turbulence Decay in the Residual Layer

When surface heating is introduced in the simulations, the residual layer, which is within the initial neutral boundary layer, becomes detached from the surface (Fig. 2). The time scale of this detachment should be representative of the formation time scale of the stable mixed layer. Previous studies of the convective atmospheric boundary layer have investigated the decay of turbulence kinetic energy components after forcing is removed (Nieuwstadt and Brost 1986; Pino et al. 2006).

Figure A1 shows the evolution of σ_w^2 with time t following the onset of a surface heat flux. The values are

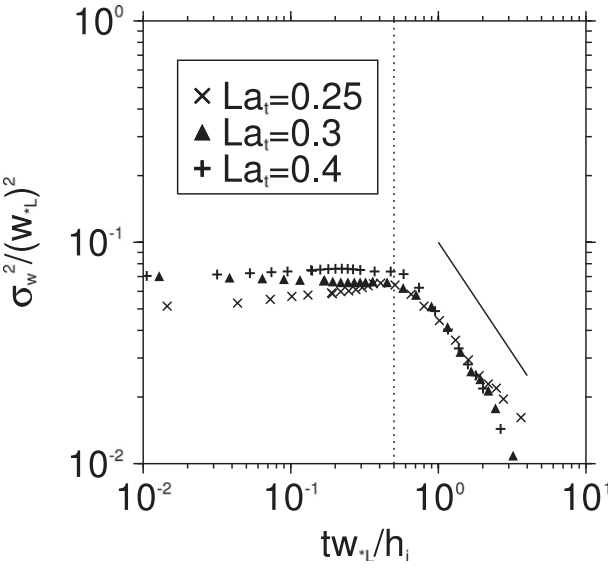

FIG. A1. Evolution of vertical velocity variance σ_w^2 with time t following the onset of surface heating at a depth of 45 m. Both axes are nondimensionalized using w_{*L} and h_i. Symbols denote the value of La_t for a given simulation. The dotted vertical line shows $tw_{*L}/h_m = 0.5$ and the solid line shows the slope of $y = x^{-1}$.

taken at a depth of 45 m, within the initial mixed layer but deeper than the equilibrium stable boundary layer. The symbols denote the Langmuir number for the simulation. Three simulations were used with $La_t = 0.25$, 0.3, and 0.4. These simulations are identical to the SM simulation with $L_L = 124$ m, except that the surface heat flux is introduced instantaneously at 50 000 s and the magnitude of u_{s0} varies between simulations to change La_t. The range of La_t can alternatively be expressed as $w_{*L} = [1.12, 1.54]\,\mathrm{cm\,s^{-1}}$. In all simulations σ_w^2 only begins to decay after $(tw_{*L}/h_i) = 0.5$ following the introduction of the surface heat flux. The vertical velocity variance then decays with time at a rate of approximately $(tw_{*L}/h_i)^{-1}$.

The response of σ_w^2 to the introduction of a surface heat flux implies that the detachment of the residual layer from the surface occurs over half a turnover time of the largest eddies, h_i/w_{*L}. In these simulations the detachment of the residual layer takes 30–40 min, and for higher wind speeds the time scale would be reduced. This time scale is much smaller than the diurnal time scale.

REFERENCES

Babanin, A., 2006: On a wave-induced turbulence and a wave-mixed upper ocean layer. *Geophys. Res. Lett.*, **33**, L20605, doi:10.1029/2006GL027308.

Belcher, S. E., and Coauthors, 2012: A global perspective on Langmuir turbulence in the ocean surface boundary layer. *Geophys. Res. Lett.*, **39**, L18605, doi:10.1029/2012GL052932.

Brainerd, K., and M. Gregg, 1993: Diurnal restratification and turbulence in the oceanic surface mixed-layer. 1. Observations. *J. Geophys. Res.*, **98**, 22 645–22 656, doi:10.1029/93JC02297.

——, and ——, 1995: Surface mixed and mixing layer depths. *Deep-Sea Res. I*, **42**, 1521–1543, doi:10.1016/0967-0637(95)00068-H.

Craik, A. D. D., and S. Leibovich, 1976: Rational model for Langmuir circulations. *J. Fluid Mech.*, **73**, 401–426, doi:10.1017/S0022112076001420.

D'Asaro, E. A., 2014: Turbulence in the upper-ocean mixed layer. *Annu. Rev. Mar. Sci.*, **6**, 101–115, doi:10.1146/annurev-marine-010213-135138.

Deardorff, J. W., 1972: Theoretical expression for the countergradient vertical heat flux. *J. Geophys. Res.*, **77**, 5900–5904, doi:10.1029/JC077i030p05900.

de Boyer Montégut, C., G. Madec, A. Fischer, A. Lazar, and D. Iudicone, 2004: Mixed layer depth over the global ocean: An examination of profile data and a profile-based climatology. *J. Geophys. Res.*, **109**, C12003, doi:10.1029/2004JC002378.

Denman, K. L., 1973: A time-dependent model of the upper ocean. *J. Phys. Oceanogr.*, **3**, 173–184, doi:10.1175/1520-0485(1973)003<0173:ATDMOT>2.0.CO;2.

Garwood, R. W., Jr., 1977: An oceanic mixed layer model capable of simulating cyclic states. *J. Phys. Oceanogr.*, **7**, 455–468, doi:10.1175/1520-0485(1977)007<0455:AOMLMC>2.0.CO;2.

Grant, A. L. M., and S. E. Belcher, 2009: Characteristics of Langmuir turbulence in the ocean mixed layer. *J. Phys. Oceanogr.*, **39**, 1871–1887, doi:10.1175/2009JPO4119.1.

——, and ——, 2011: Wind-driven mixing below the oceanic mixed layer. *J. Phys. Oceanogr.*, **41**, 1556–1575, doi:10.1175/JPO-D-10-05020.1.

Harcourt, R. R., and E. A. D'Asaro, 2008: Large-eddy simulation of Langmuir turbulence in pure wind seas. *J. Phys. Oceanogr.*, **38**, 1542–1562, doi:10.1175/2007JPO3842.1.

Holtslag, A. A. M., and C.-H. Moeng, 1991: Eddy diffusivity and countergradient transport in the convective atmospheric boundary layer. *J. Atmos. Sci.*, **48**, 1690–1698, doi:10.1175/1520-0469(1991)048<1690:EDACTI>2.0.CO;2.

Kukulka, T., A. J. Plueddemann, and P. P. Sullivan, 2013: Inhibited upper ocean restratification in nonequilibrium swell conditions. *Geophys. Res. Lett.*, **40**, 3672–3676, doi:10.1002/grl.50708.

Large, W. G., J. C. McWilliams, and S. C. Doney, 1994: Oceanic vertical mixing: A review and a model with a nonlocal boundary layer parameterization. *Rev. Geophys.*, **32**, 363–403, doi:10.1029/94RG01872.

Li, M., C. Garrett, and E. Skyllingstad, 2005: A regime diagram for classifying turbulent large eddies in the upper ocean. *Deep-Sea Res. I*, **52**, 259–278, doi:10.1016/j.dsr.2004.09.004.

McWilliams, J. C., P. P. Sullivan, and C. H. Moeng, 1997: Langmuir turbulence in the ocean. *J. Fluid Mech.*, **334**, 1–30, doi:10.1017/S0022112096004375.

Min, H., and Y. Noh, 2004: Influence of the surface heating on Langmuir circulation. *J. Phys. Oceanogr.*, **34**, 2630–2641, doi:10.1175/JPOJPO-2654.1.

Monin, A. S., and A. M. Obukhov, 1954: Basic laws of turbulent mixing in the surface layer of the atmosphere. *Tr. Geofiz. Inst., Akad. Nauk SSSR*, **24**, 163–187.

Nieuwstadt, F., and R. Brost, 1986: The decay of convective turbulence. *J. Atmos. Sci.*, **43**, 532–546, doi:10.1175/1520-0469(1986)043<0532:TDOCT>2.0.CO;2.

Noh, Y., H. Min, and S. Raasch, 2004: Large eddy simulation of the ocean mixed layer: The effects of wave breaking and Langmuir

circulation. *J. Phys. Oceanogr.*, **34**, 720–735, doi:10.1175/1520-0485(2004)034<0720:LESOTO>2.0.CO;2.

——, G. Goh, S. Raasch, and M. Gryschka, 2009: Formation of a diurnal thermocline in the ocean mixed layer simulated by LES. *J. Phys. Oceanogr.*, **39**, 1244–1257, doi:10.1175/2008JPO4032.1.

Paulson, C. A., and J. J. Simpson, 1977: Irradiance measurements in the upper ocean. *J. Phys. Oceanogr.*, **7**, 952–956, doi:10.1175/1520-0485(1977)007<0952:IMITUO>2.0.CO;2.

Pino, D., H. J. Jonker, J. V.-G. De Arellano, and A. Dosio, 2006: Role of shear and the inversion strength during sunset turbulence over land: Characteristic length scales. *Bound.-Layer Meteor.*, **121**, 537–556, doi:10.1007/s10546-006-9080-6.

Plueddemann, A. J., and R. A. Weller, 1999: Structure and evolution of the oceanic surface boundary layer during the surface waves processes program. *J. Mar. Syst.*, **21**, 85–102, doi:10.1016/S0924-7963(99)00007-X.

Polton, J. A., and S. E. Belcher, 2007: Langmuir turbulence and deeply penetrating jets in an unstratified mixed layer. *J. Geophys. Res.*, **112**, C09020, doi:10.1029/2007JC004205.

Price, J., R. Weller, and R. Pinkel, 1986: Diurnal cycling - Observations and models of the upper ocean response to diurnal heating, cooling, and wind mixing. *J. Geophys. Res.*, **91**, 8411–8427, doi:10.1029/JC091iC07p08411.

Rossby, C.-G., and R. B. Montgomery, 1935: The layer of frictional influence in wind and ocean currents. *Papers in Physical Oceanography and Meteorology*, Vol. 3, No. 3, 101 pp., doi:10.1575/1912/1157.

Shutts, G. J., and M. E. B. Gray, 1994: A numerical modelling study of the geostrophic adjustment process following deep convection. *Quart. J. Roy. Meteor. Soc.*, **120**, 1145–1178, doi:10.1002/qj.49712051903.

Skyllingstad, E., and D. Denbo, 1995: An ocean large-eddy simulation of Langmuir circulations and convection in the surface mixed layer. *J. Geophys. Res.*, **100**, 8501–8522, doi:10.1029/94JC03202.

Stokes, G. G., 1847: On the theory of oscillatory waves. *Trans. Cambridge Philos. Soc.*, **8**, 441–463.

Sullivan, P. P., J. C. McWilliams, and W. K. Melville, 2007: Surface gravity wave effects in the oceanic boundary layer: Large-eddy simulation with vortex force and stochastic breakers. *J. Fluid Mech.*, **593**, 405–452, doi:10.1017/S002211200700897X.

Sutherland, G., B. Ward, and K. Christensen, 2013: Wave-turbulence scaling in the ocean mixed layer. *Ocean Sci.*, **9**, 597–608, doi:10.5194/os-9-597-2013.

——, K. Christensen, and B. Ward, 2014: Evaluating Langmuir turbulence parameterizations in the ocean surface boundary layer. *J. Geophys. Res.*, **119**, 1899–1910, doi:10.1002/2013JC009537.

Teixeira, M. A. C., and S. E. Belcher, 2002: On the distortion of turbulence by a progressive surface wave. *J. Fluid Mech.*, **458**, 229–267, doi:10.1017/S0022112002007838.

——, and ——, 2010: On the structure of langmuir turbulence. *Ocean Modell.*, **31**, 105–119, doi:10.1016/j.ocemod.2009.10.007.

Zilitinkevich, S. S., 1972: On the determination of the height of the Ekman boundary layer. *Bound.-Layer Meteor.*, **3**, 141–145, doi:10.1007/BF02033914.

——, and A. Baklanov, 2002: Calculation of the height of the stable boundary layer in practical applications. *Bound.-Layer Meteor.*, **105**, 389–409, doi:10.1023/A:1020376832738.

——, ——, J. Rost, A.-S. Smedman, V. Lykosov, and P. Calanca, 2002: Diagnostic and prognostic equations for the depth of the stably stratified Ekman boundary layer. *Quart. J. Roy. Meteor. Soc.*, **128**, 25–46, doi:10.1256/00359000260498770.